Materials Today Communications 2 (2015) e38–e48

Contents lists available at ScienceDirect

Materials Today Communications

journal homepage: www.elsevier.com/locate/mtcomm

A possible scalable method for the synthesis of Sn-containing carbon nanostructures

Ali Reza Kamali*, Derek J. Fray

Department of Materials Science and Metallurgy, University of Cambridge, 27 Charles Babbage Road, Cambridge CB3 0FS, UK

ARTICLE INFO

Article history:
Received 23 November 2014
Accepted 24 November 2014
Available online 5 December 2014

Keywords:
Carbon nanotubes
Nanoparticles
Tin-encapsulated carbon
Tin oxide
LiCl
$SnCl_2$

ABSTRACT

This paper presents a scalable and efficient method for the preparation of Sn-containing carbon nanostructures, based on the cathodic erosion of graphite electrodes in molten LiCl–$SnCl_2$ salt mixture. The product obtained was characterized by means of X-ray diffraction and electron microscopy. It was found that conducting the process in nominally pure argon containing a low concentration of oxygen leads to the formation of Sn-encapsulated carbon nanostructures as well as SnO_2-decorated carbon nanotubes (CNTs). On the other hand, CNTs decorated with SnO_2 nanocrystals could be synthesized in high yield in the presence of higher concentrations of oxygen. The oxidation of $SnCl_2$ to SnO_2 nanocrystals was found to be both thermodynamically and kinetically possible in atmospheres containing very small quantities of oxygen and to avoid the formation of tin oxides, it was necessary to perform the process under reducing conditions. The tin nanostructures encapsulated in carbon shells were found to be stable upon washing with water and drying. The results obtained provide essential knowledge to control the molten salt process.

© 2014 Elsevier Ltd. All rights reserved.

1. Introduction

Polycrystalline synthetic graphite (so-called graphite) can be corroded in molten alkali metal halides to form carbon nanostructures with a high degree of graphitization [1–4]. The corrosion/erosion of graphite in molten salts can be enhanced when a cathodic potential is applied to the graphite which makes the electrolytic conversion of graphite an attractive and economically viable emerging technology for the preparation of carbon nanomaterials. Using this method, the erosion product is in the form of CNTs and carbon nanoparticles which can be retrieved from the solidified salt by washing and filtering. An attractive feature of this technology is that CNTs and spherical nanoparticles can be produced by appropriately controlling the process parameters including the microstructural properties of graphite feed materials and electrolysis condition [5–11]. The molten salt approach was recently modified to develop a convenient and scalable process for reliable preparation of carbon nanostructures, in which the production rate could reach to 10 g h^{-1} by cathodic polarization of a graphite rod of 15 mm in diameter, immersed in molten LiCl. The method presented could be easily scaled up to provide significant quantities of carbon nanostructures [11].

Another attractive feature of the molten salt process is its capability of producing filled carbon nanomaterials, in which a metallic second phase is encapsulated by graphitic carbon. For example, Sn-filled carbon nanostructures have been produced by heating a mixture of LiCl and $SnCl_2$ to a temperature greater than 700 °C, followed by electrolysis of the molten salt using graphite electrodes. The cathodic reactions that occurred during the electrolysis can be described as follows: (a) Sn^{2+} ions are first reduced to Sn on the surface of the graphite cathode, (b) Li^+ is reduced at the graphite cathode to form carbon intercalation compound or carbon-Li intermediate phases, (c) sheets of graphite are extruded which encapsulate the tin to form tin-encapsulated carbon nanostructures. When cooled down, the solidified salt can be washed off by distilled water and the carbonaceous product retrieved [12–15]. The material produced by this method was examined as anode material for lithium-ion batteries, and showed a promising electrochemical performance [16].

It should be noted that tin-filled carbon nanostructures with enhanced anode performances in lithium ion batteries have also been fabricated via various other methods including chemical vapor deposition [17–20], capillary-loading [21] sol–gel [22], ion exchange [23], aerosol spray pyrolysis [24,25] and electrospinning [26].

* Corresponding author. Tel.: +44 1223 334300.
E-mail address: ark42@cam.ac.uk (A.R. Kamali).

http://dx.doi.org/10.1016/j.mtcomm.2014.11.001
2352-4928/© 2014 Elsevier Ltd. All rights reserved.

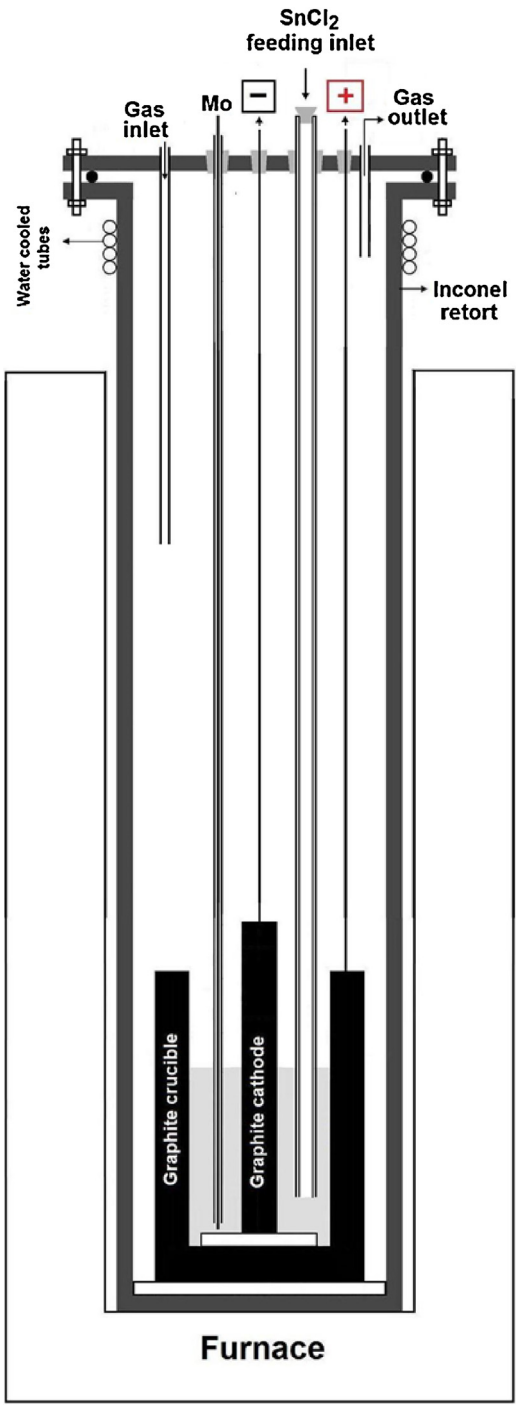

Fig. 1. Schematic representation of the experimental set-up used for the large-scale preparation of Sn-containing carbon nanomaterials in molten LiCl. It includes a graphite rod immersed in molten LiCl, which is used as the cathode during the electrolysis process, and a graphite crucible which is used as the anode. $SnCl_2$ pellets could be introduced into the molten LiCl through the alumina tube shown at different intervals during the electrolysis.

Fig. 2. Photographs of a graphite rod (a) before and (b) after being used as the cathode during the electrolysis of LiCl-30 wt% $SnCl_2$. The molten salt electrolysis was conducted at 770 °C for 2 h at the constant current of 33 A, corresponding to an initial cathode current density of about 1 A cm^{-2}. Details of the set-up used can be found in [11].

The molten salt technology, however, offers a much faster and perhaps more economic route for the preparation of Sn-filled carbon nanomaterials, in comparison with the other available methods [27]. Despite the interesting features of the molten salt process, some main issues need attention before the process can be successfully scaled-up.

First, it has been found that the above-described process may lead to the formation of Sn-filled carbon nanostructures if, and only if, the $SnCl_2$ content of the initial salt mixture is less than about 2 wt%. At higher concentrations of $SnCl_2$, the formation of carbon product is completely suppressed which was attributed to the excessive deposition of Sn on the electrodes restricting the access of Li^+ ions from the melt to the graphite, which suppresses the erosion of graphite cathodes and the formation of nanostructured carbon product. Furthermore, it was found that only 1 g carbon product, containing 16 wt% Sn, could be produced during 25 min electrolysis using graphite electrodes of 6.5 mm diameter in a salt mixture containing 200 g LiCl and 2 g $SnCl_2$ [15]. It is obvious that the process needs to be modified if it is to be considered as a method for the production of tin-filled carbon nanostructures. Two issues are addressed in this paper: the continuous addition of tin chloride to the melt and the avoidance of the creation of tin oxide during the process as these oxide phases have a detrimental effect on the performance of lithium ion batteries.

It should be noted that carbonaceous product fabricated by the electrolysis of molten LiCl–$SnCl_2$ in argon atmosphere contained a considerable amount of tin oxides as well as a minor amount of Li_2SnO_3 in addition to carbon and tin [15]. In the literature, the formation of SnO_2 has been solely attributed to the hypothesis that Sn inside the cavity of carbon nanostructures partly reacts with oxygen during washing, drying or storage to form SnO_2 [15]. This hypothesis, however, needs to be explored as it does not take into account the reactions which may take place during heating the mixture of LiCl and $SnCl_2$ from room temperature to high temperatures in laboratory grade argon. Furthermore, carbon layers usually provide an effective barrier against oxidation of the encapsulated metals. In fact, no oxidation of Sn was observed even after six months of exposure to air of Sn-filled CNTs [28].

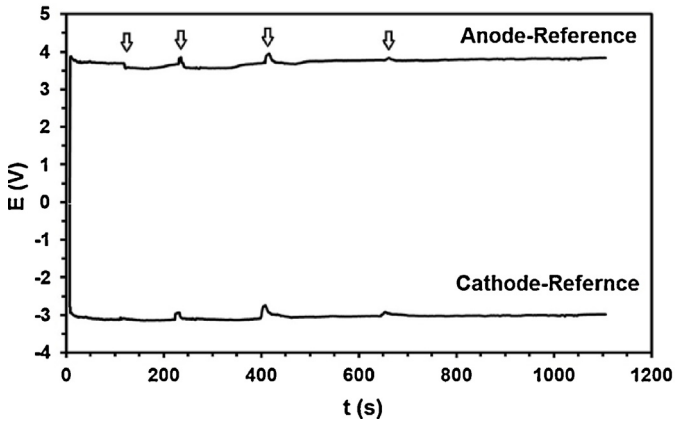

Fig. 3. The potential difference between the graphite electrodes (anode and cathode) and a Mo pseudo-reference electrode immersed in the molten salt. Addition of $SnCl_2$ pellets to the molten salt during the electrolysis caused individual waves on the curves. The voltage values recorded included 1.2 V, the potential drops across the length of two SS electrical connectors.

Although the electrochemical formation of Sn-filled carbon nanostructures has been subjected to comprehensive investigations [12–15], the possible phase transitions within the molten salt have been disregarded in previous studies. The controllability of the process is indeed deteriorated in the absence of this knowledge.

Thus, another purpose of the current paper is to study the thermal phase transitions that may occur in LiCl–$SnCl_2$ mixture, shedding light on the mechanism of oxide formation in this molten salt system.

2. Experimental

2.1. Preparation of Sn-containing carbon nanostructures

A scalable fabrication method for the preparation of carbon nanostructures in molten LiCl was discussed in our pervious study [11]. Briefly, the experimental set-up consists of a graphite crucible containing sufficient amount of LiCl which is positioned in a gas-tight Inconel retort. The crucible is heated to the target temperature of about 770 °C under an atmosphere of argon. At the target temperature, a graphite rod immersed in molten salt is subjected to cathodic polarization providing a cathode current density of about 1 A cm^{-2}, while the graphite crucible serves as the anode. During the electrolysis, graphite cathode is eroded, and the erosion product detached from the graphite electrode is dispersed throughout the molten salt. After cooling down to room temperature, the salt can be washed off and the carbon product retrieved. In the current study, the set-up of the previous study [11] was equipped with an alumina tube which was used for continuous addition of $SnCl_2$ to molten LiCl. Fig. 1 shows a schematic drawing of the experimental set-up used for this study.

A QPX600DP Dual 600Watt power supply was employed to provide the current during electrolysis. Nominally anhydrous LiCl powders (213233, Sigma–Aldrich), $SnCl_2$ flake-like particles (208256, Sigma–Aldrich), graphite rods with a mean grain size 150 μm and a diameter of 15 mm (Morgan AM&T, electrical grade graphite purity 99.99%), and a graphite crucible of inner diameter 57 mm and height 130 mm were used in this investigation.

2.2. Characterization of products

The morphology and crystal structure of products obtained were examined by a JEOL 6340F field emission scanning electron microscope (SEM), a FEI Nova Nano-SEM, a 200 kV JEOL 2000FX analytical transmission electron microscope (TEM) equipped with selected area electron diffraction, and a FEI Tecnai F20. A Philips 1710 X-ray diffractometer (XRD) with Cu-K_α radiation (k = 1.54 A°) was used to record the diffraction patterns. XRD data were analyzed using the X'Pert High Score Plus program.

In order to examine the thermal stability of the salts, thermal analyses were conducted by means of non-isothermal differential scanning calorimetry (DSC) and thermogravimetry (TG) using an SDT Q600 analyser equipped with alumina crucibles. Thermodynamic data of selected reactions were calculated using a commercial software package [29].

3. Results and discussion

It has been known that the electrolysis of LiCl containing a small amount of $SnCl_2$ using graphite electrodes leads to the formation of a small quantity of Sn-filled carbon nanostructures, whilst any concentration of greater than 2 wt% $SnCl_2$ prevents the formation of carbon nanostructures [12–16]. Fig. 2 shows photographs of a graphite rod before and after being used as the cathode during the electrolysis of LiCl containing an initial $SnCl_2$ concentration of

Fig. 4. The graphite electrode used as the cathode was gradually eroded, whilst $SnCl_2$ pellets were fed into the molten salt at different intervals during the electrolysis process. This figure shows the photographs of the graphite rod (a) before and after being used as cathode in the process for (b) 20 min and (c) 2 h, when 20 g and 85 g $SnCl_2$ was added to molten LiCl, respectively. (d) The solidified salt inside the graphite crucible and (e) the final product (about 20 g) obtained after 2 h of electrolysis.

30 wt%. As shown, only a minor erosion could be observed on the electrode. On the other hand, since the Sn electrodeposited on the graphite electrode (with a melting point of 232 °C) was in a molten state at the temperature of the process (about 800 °C), it then sank in the molten salt to the bottom of the crucible due to its higher density, which allowed the formation of a Sn disk at the bottom of the rod after cooling down to room temperature, as can be seen in Fig. 2.

3.1. Efficient preparation of Sn-containing carbon nanostructures

An efficient method for the preparation of Sn-containing carbon nanostructures was employed in this study in which $SnCl_2$ is continuously added to molten LiCl during the electrolysis process. For this purpose, $SnCl_2$ powders were pressed into cylindrical pellets of 10 mm diameter under about 200 MPa pressure for few seconds in a steel mold using a manual hydraulic press. The green body strength of pellets was high enough for handling of the pellets during the molten salt process. The cell, shown in Fig. 1, used 250 g LiCl, and the electrolysis was conducted under galvanostatic condition with the constant current of 33 A in a flow of nominally pure Ar containing an oxygen content of about 20 ppm. Four $SnCl_2$ pellets, each about 5 g, were introduced into the molten salt at different intervals during the electrolysis. The potential difference between the graphite electrodes (anode and cathode) and a Mo pseudo-reference electrode immersed in the molten salt is shown in Fig. 3. The potential differences were measured by connecting two stainless steel (SS) connectors of 6 mm in diameter and the Mo wire reference electrode to a digital multimeter (Agilent 34405A). The voltage values recorded included 1.2 V, the potential drops across the length of SS connectors [11]. The $SnCl_2$ pellets were dropped into molten salt from the upper end of an alumina tube as shown in Fig. 1. Addition of $SnCl_2$ pellets might cause individual waves on the *E–t* curves, shown by arrows in Fig. 3. After about 20 min of electrolysis, the reactor was allowed to be cooled down to room temperature. It was observed that the solidified salt had become black in appearance, indicating that the graphite rod was eroded and the erosion material was mixed with salt. The content of the graphite crucible was repeatedly washed with distilled water in order to dissolve LiCl and the suspension obtained was filtered through filter paper. The material obtained was then dried in an oven at 100 °C for 10 h, resulting in about 5 g black colored powder, which was characterized by means of XRD, SEM and TEM, explained in the following sections. The appearance of the graphite rod before and after being used as the cathode during the electrolysis is shown in Figs. 4a and b, confirming the occurrence of a slight and uniform erosion of the graphite rod immersed in molten LiCl.

It should be noticed that the erosion of graphite cathodes is suppressed if $SnCl_2$ is pre-added into LiCl in quantities more than 2 wt% [15,16]. As shown in this paper, a quantity of greater than 7 wt% $SnCl_2$ was gradually added to molten LiCl during the electrolysis, and an effective erosion of the graphite rod could be still obtained. The same procedure was repeated to add 15, 20 and 30 wt% $SnCl_2$ to the molten salt, while a good erosion yield was achieved. For example, Fig. 4c shows the appearance of the graphite rod after being used as the cathode for 2 h, whilst 30 wt% $SnCl_2$ was added to the molten salt. In this case 20 g product containing 50 wt% Sn was obtained (Figs. 4d and e). The results are of special interest as it demonstrates the potential of the process for large-scale synthesis of Sn-filled carbon nanostructures.

3.2. Characterization of the Sn-containing carbon nanostructures produced

The products obtained by 20 min electrolysis of molten LiCl and gradually added $SnCl_2$ in different atmospheres were characterized by XRD, SEM and TEM. The XRD pattern of the product obtained in Ar containing 20 ppm O_2 (Fig. 5a) is characterized by the diffraction peaks of C, Sn, LiCl and SnO_2. LiCl peaks indicate that residual LiCl remains trapped in the product after electrolysis and washing. It should be noticed that LiCl easily absorbs moisture from the environment to form lithium chloride hydrates [30]. The anhydrous nature of the LiCl in the product confirms that LiCl is encapsulated in carbon nanostructures and therefore is protected from environment as discussed more detailed in [31]. In addition to LiCl, the peaks of Sn and SnO_2 can also be observed in the pattern. The formation of Sn, which is due to the discharge of Sn^{2+} cations on the graphite cathode surface during the electrolysis process, has been the subject of several studies [12–16]. It is generally believed that metallic Sn formed during the molten salt process can be encapsulated within the carbon nanostructures. In agreement with these investigations, electron microscopy examinations of the sample produced in this study revealed the presence of Sn within carbon nanostructures, as can be seen in Fig. 6.

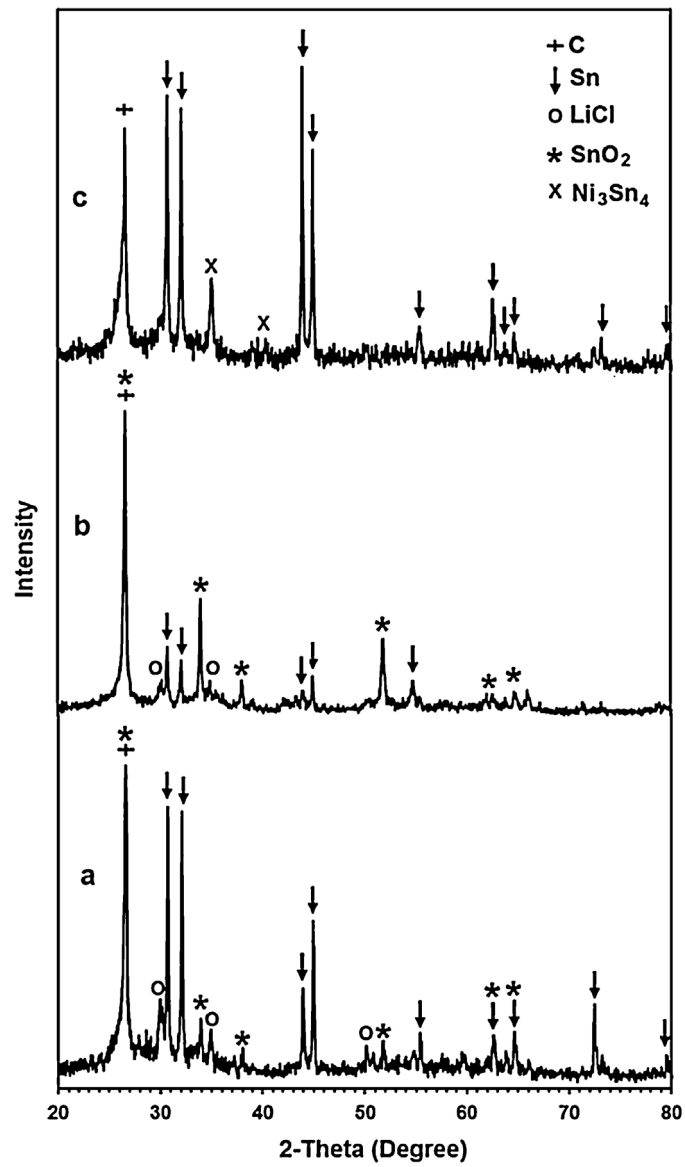

Fig. 5. XRD analysis of the sample obtained by 20 min electrolysis of molten LiCl – gradually added $SnCl_2$ using the set-up explained in Fig. 1 in (a) nominally pure Ar containing 20 ppm O_2, (b) Ar–2% O_2 and (c) Ar–4% H_2 gas flow.

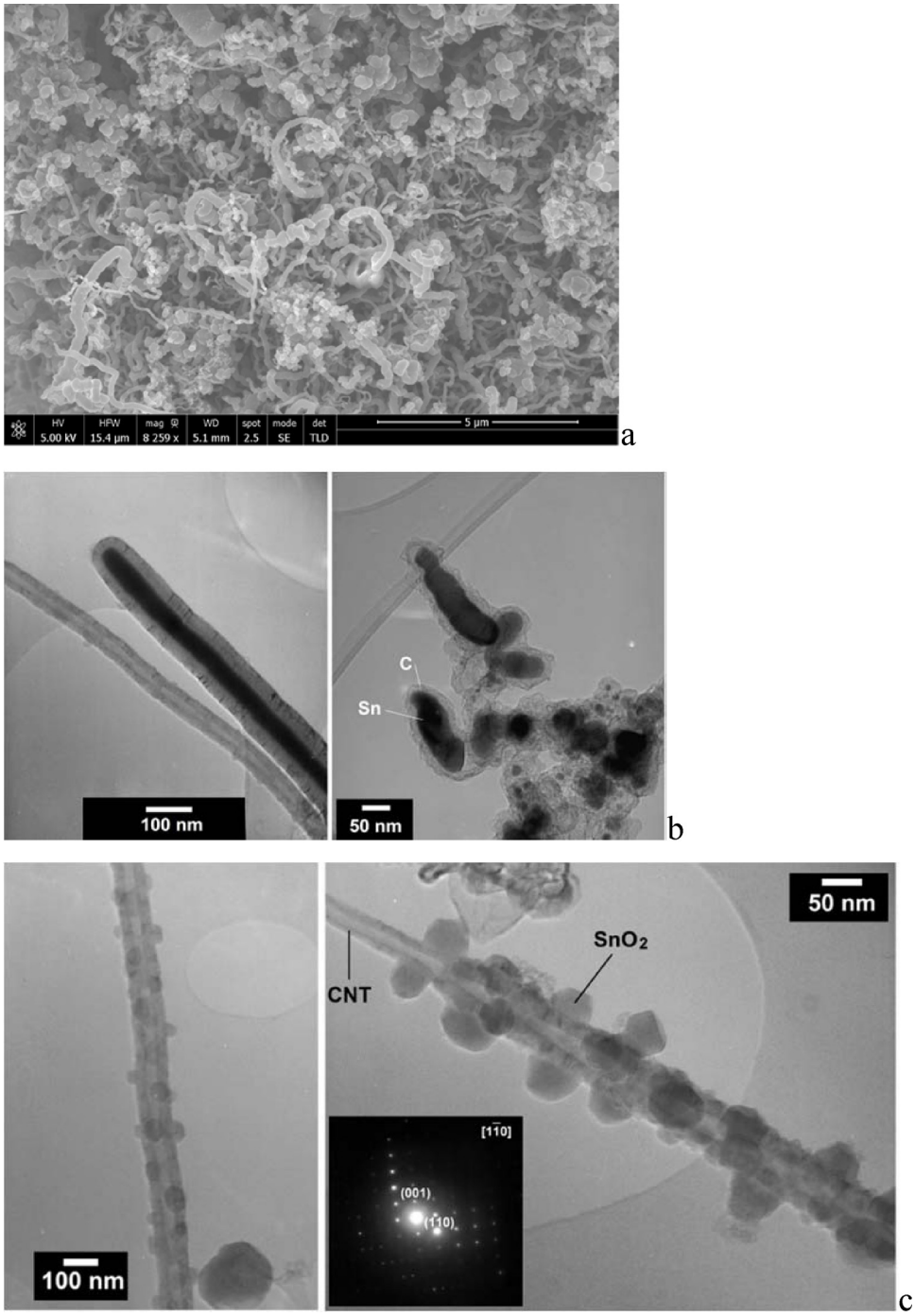

Fig. 6. EM images of the sample prepared by 20 min electrolysis of molten LiCl – gradually added $SnCl_2$ in nominally pure Ar containing 20 ppm O_2 as explained in Figs. 1, 3 and 4. (a) A SEM image showing the presence of nanostructures including CNTs and carbon nanoparticles. (b) and (c) Show bright field TEM images taken from different locations on the sample. The microstructural features observed included (b – left panel) Sn-filled and empty CNTs, (b – right panel) Sn-filled carbon nanoparticles, and (c) SnO_2-decorated CNTs. The inset in (c) is a selected area diffraction pattern from an individual SnO_2 nanocrystal.

SEM analyses, such as shown in Fig. 6a, showed that the sample obtained after 20 min of electrolysis mainly consisted of either tubular or spherical nanostructures with dimensions typically less than 100 nm. Figs. 6b and c exhibit bright field TEM images taken from different locations of the sample. The left hand panel in Fig. 6b shows two CNTs. The central cavity of one of the tubes (with outer diameter of about 100 nm) is filled with Sn while the other one (with outer diameter of about 50 nm) is empty. The right hand panel in Fig. 6b presents a core–shell nanostructure in which Sn is encapsulated inside carbon shells. It should be mentioned that the Sn nature of the filling material in these core–shell nanostructures was confirmed using EELS measurements. For example, Fig. 7 shows a STEM image recorded on a partially filled carbon nanotube, and EELS spectra measured at the filled and empty area of the tube. The spectrum measured at the empty area of the CNT reveals the presence of C K-shell ionization edge at approximately 24 eV, while the spectra recorded on the filled areas show the presence of the C K- and Sn $M_{4,5}$-shell ionization edges at approximately 24 and 27 eV, respectively. The results confirm the core–shell morphology of Sn–C nanostructures formed.

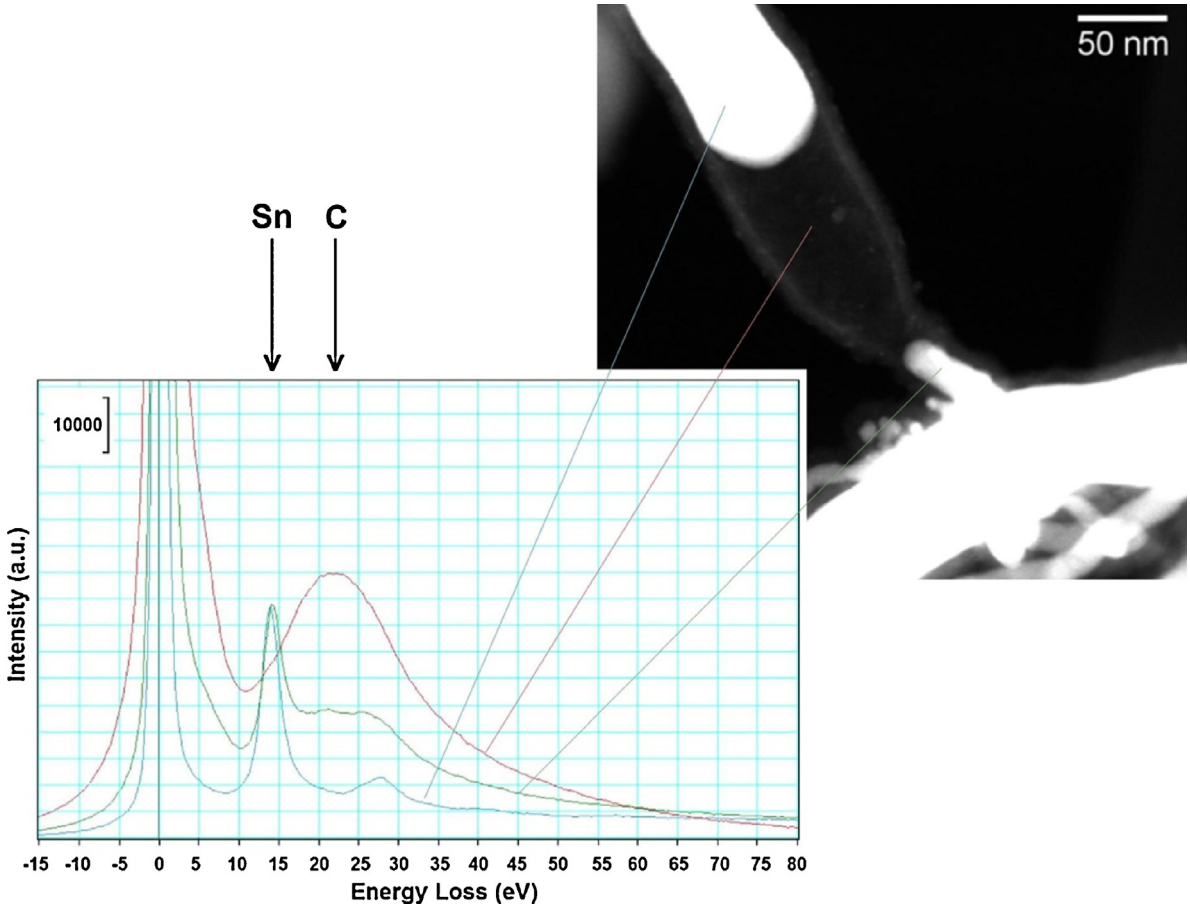

Fig. 7. STEM image of a partially filled carbon nanotube, and EELS spectra measured at the filled and empty areas of the tube, confirming the core–shell morphology of Sn–C nanostructures formed.

On the other hand, besides the peaks of C, Sn and LiCl, the reflection peaks of SnO_2 are also observed in the XRD pattern of the sample prepared by 20 min electrolysis of molten LiCl – gradually added $SnCl_2$ in nominally pure Ar containing 20 ppm O_2 – as shown in Fig. 5a. The formation of tin oxide during the molten salt synthesis of Sn-filled carbon nanostructures has also been reported in the literature [15,16], although no investigation was conducted on the morphology of this phase. In the current study, the morphology of the SnO_2 component was confirmed by careful TEM characterization. The TEM micrographs, shown in Fig. 6c, together with selected area diffraction pattern analyses (such as the inset of Fig. 6c) revealed that SnO_2 is present in the product in the form of nano-single crystals which are attached to the external surfaces of CNTs. This morphological feature may be especially promising for applications such as chemical sensors [32] and energy storage materials [33].

However, the knowledge of the mechanisms involved in the formation of SnO_2 phase during the molten salt process of the preparation of Sn-containing carbon nanostructures is obviously vital for the future development of the technology, enabling one to control the formation of SnO_2 nanocrystals.

3.3. *Mechanism of oxide formation in LiCl–$SnCl_2$ molten salt*

As explained, the Sn-encapsulated carbon nanostructures prepared in LiCl–$SnCl_2$ molten salt may contain SnO_2 and also Li_2SnO_3 [15]. In order to understand the mechanism behind the formation of these phases, the thermal phase transitions of $SnCl_2$ and LiCl were studied.

3.3.1. *Thermal phase transitions of $SnCl_2$*

In order to study the thermal behavior of tin chloride, 50–90 mg $SnCl_2$ was thermal analyzed by means of DSC and TG at the heating rate of 10 and 40 °C min^{-1}, under both Ar and air flow of 100 mL min^{-1}. The results are shown in Fig. 8, and the specific peak temperatures for the various phase transitions of $SnCl_2$ are summarized in Table 1. The thermal behavior of $SnCl_2$ in a flow of air has been already reported in our recent studies [34–36]. As shown in Fig. 8 and Table 1, heating of $SnCl_2$ at 10 °C min^{-1} in air led to the melting of the material characterized by an endothermic peak at 255 °C. The second endothermic peak that appeared at 507 °C is attributed to the partial evaporation of molten $SnCl_2$. However, the $SnCl_2$ evaporation is not complete, and the evaporation peak is immediately followed by an exothermic peak at 531 °C, which is due to the oxidation of the remaining molten $SnCl_2$ [36]. On the other hand, as can be seen from Fig. 8 and Table 1, $SnCl_2$ melts at an identical temperature of 255 °C when heated at 10 °C min^{-1} in Ar. Moreover, the evaporation peak of the $SnCl_2$ material is detected at 528 °C, followed by the oxidation peak at 561 °C. This result is

Table 1
The values of peak position (°C) for melting, vaporization, and oxidation of $SnCl_2$ at different heating rates and atmospheres, obtained from DSC curves of Fig. 8.

Heating rate (°C min^{-1})		Melting	Vaporization	Oxidation
10	Air	255	507	531
	Ar	255	528	561
40	Air	269	567	>567
	Ar	270	585	>585

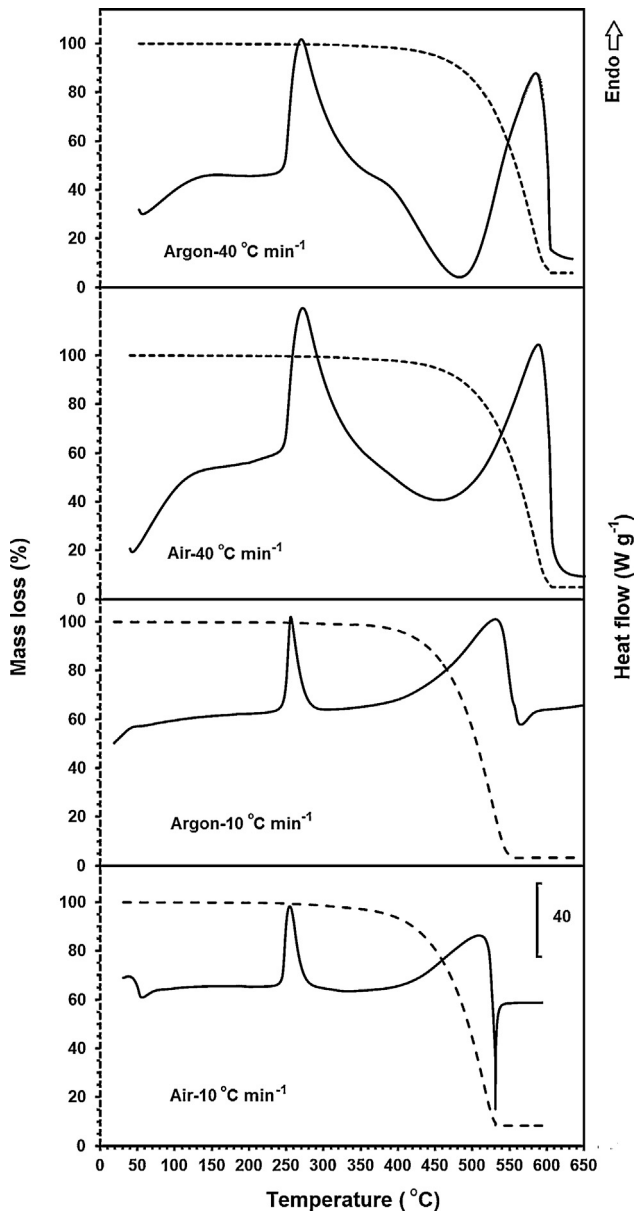

Fig. 8. DSC (sold lines) and TG (dotted lines) curves for 50–90 mg of $SnCl_2$ heated at different heating rates and atmospheres. The measurements were conducted in an ambient gas flow of 100 mL min^{-1}.

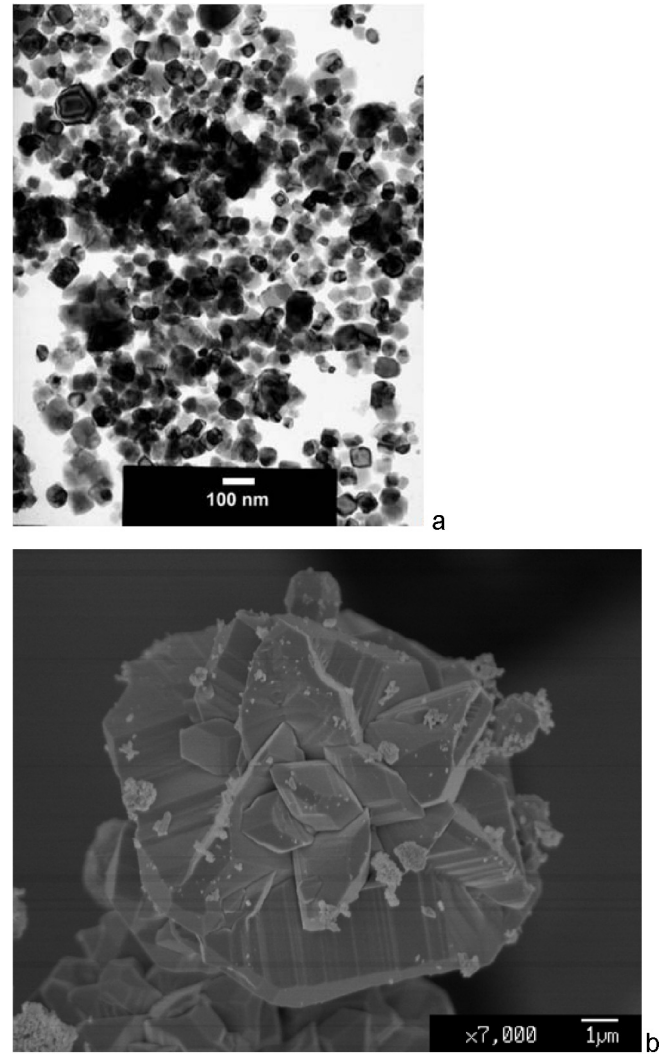

Fig. 9. (a) Bright field TEM micrograph of SnO_2 nanoparticles obtained by heating of $SnCl_2$ at 600 °C at the heating rate of 10 °C min^{-1} in a flow of Ar gas. The SnO_2 nanocrystals grow to large sizes of several micrometers upon further heating to 800 °C, as observed in (b).

important because it suggests that $SnCl_2$ can be oxidized even when the material is heated in a flow of nominally pure argon. As will be explained later in this paper, the occurrence of oxidation reaction can be attributed to the presence of small quantities of oxygen in the argon gas used. As can be depicted, the evaporation and oxidation in Ar of $SnCl_2$ takes place at higher temperature than those in air. The lower temperature of the oxidative vaporization in air of $SnCl_2$ can be attributed to the higher activity of oxygen in air in comparison to that of Ar gas.

As seen in Fig. 8 and Table 1, melting of $SnCl_2$ at the heating rate of 40 °C min^{-1} takes place at 269 and 270 °C in a flow of air and Ar, respectively. Likewise observed at 10 °C min^{-1}, whilst the melting temperature of $SnCl_2$ at 40 °C min^{-1} is almost independent of the atmosphere, vaporization temperature of $SnCl_2$ in Ar (585 °C) is considerably higher than that of in air (567 °C).

It has been demonstrated [36] that at the heating rates equal or lower than 10 °C min^{-1}, the oxidation in air of $SnCl_2$ molten salt happened by a liquid–solid (LS) phase transition during the evaporation event leading to the appearance of an exothermic peak on the corresponding DSC curves, as seen in Fig. 8. At higher heating rates, however, the formation of SnO_2 is caused by the oxidation of $SnCl_2$ vapour through a gas–solid (GS) phase transition, leaving no peak on the corresponding DSC curve [36]. It can be seen from Fig. 8 that heating of $SnCl_2$ in Ar causes the same phase changes as in air. TG curves of Fig. 8 confirms that evaporation of $SnCl_2$ in both air and Ar does not proceed to complete loss of the material, and continued by an oxidation process leading to leave a small mass behind.

Fig. 9a shows bright field TEM micrograph of SnO_2 nanoparticles obtained by heating of $SnCl_2$ to 600 °C at the heating rate of 10 °C min^{-1} in a flow of Ar gas. Likewise the material produced in air flow [35], the morphology of the material formed in Ar can be characterized by the presence of SnO_2 nanocrystals of mostly less than 100 nm. The SnO_2 nanocrystals grow to large sizes of several micrometers upon further heating to 800 °C, as observed in Fig. 9b.

The results shown in Figs. 8 and 9 imply that $SnCl_2$ undergoes oxidation during heating at heating rates of 10 and 40 °C min^{-1} in a flow of Ar gas according to reactions (1) and (2), respectively.

$$[SnCl_2]_{solid} \xrightarrow{255\,^{\circ}C} [SnCl_2]_{liquid} \xrightarrow{528-561\,^{\circ}C} [SnCl_2]_{gas} + [SnO_2]_{solid} \quad (1)$$

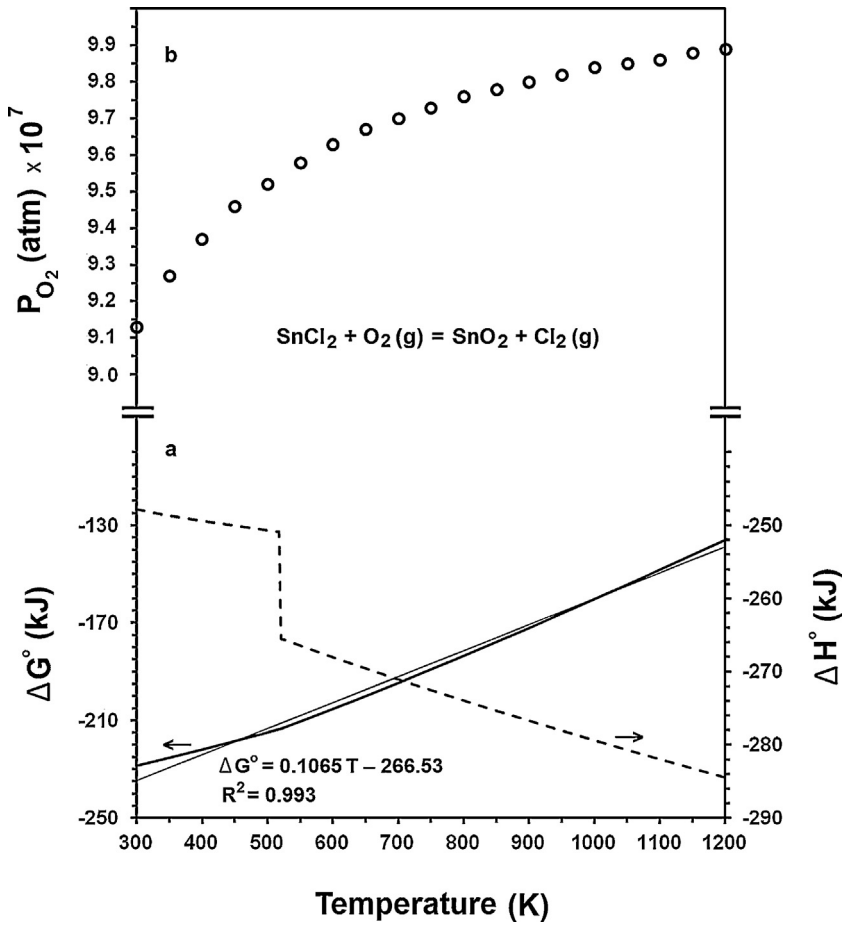

Fig. 10. (a) Changes in the standard Gibbs free energy and the standard enthalpy of the reaction (3) against temperature. A linear fitting of the ΔG–T data can also be observed. (b) Values of the equilibrium oxygen partial pressure of the reaction (3) against temperature.

$$[SnCl_2]_{solid} \xrightarrow{270\,^\circ C} [SnCl_2]_{liquid} \xrightarrow{585\,^\circ C} [SnCl_2]_{gas} \xrightarrow{T>585\,^\circ C} [SnCl_2]_{solid} \quad (2)$$

A question which may be raised is the possibility of the oxidation of $SnCl_2$ in nominally pure Ar gas.

Fig. 10a shows changes in the standard Gibbs free energy and the standard enthalpy of the reaction (3) against temperature, calculated using a commercial software package [29].

$$SnCl_2 + O_2 = SnO_2 + Cl_2 \quad (3)$$

The values of ΔG° versus T for the reaction (3) are shown in Fig. 10a. Assuming Sn and SnO_2 are pure and the partial pressure of Cl_2 in the reactor is 1 ppm, it is possible to calculate the equilibrium partial pressure of oxygen and this is shown in Fig. 10b. It confirms that an oxygen concentration of greater than 1 ppm is thermodynamically sufficient to cause the oxidation of $SnCl_2$ to SnO_2.

3.3.2. *Thermal phase transitions in LiCl–$SnCl_2$ mixture*

A mixture of LiCl with 30 wt% $SnCl_2$ (total weight of 10 g) was placed in an alumina crucible. The crucible was placed in a tube furnace and heated at 200 °C for 10 h under a flow of Ar to remove the crystalline water of the salts. Then the temperature was raised to 800 and 1300 °C at the heating rate of 10 °C min^{-1} with a dwelling time of 1 h, and after that the furnace was cooled down under the same gas flow. At the ambient temperature, the solidified salt which was firmly attached to the crucible was washed with distilled water to dissolve salts, and the solution obtained was vacuum filtered using a Buchner funnel and filter paper. A small quantity of white powder was found on the filter paper. This powder was dried and analyzed to identify its nature and morphology.

The XRD pattern of the powder obtained at 800 °C is shown in Fig. 11a, revealing that the material is single phase SnO_2 with rutile structure. This result is important because it shows that SnO_2 is formed during heating of LiCl–$SnCl_2$ mixture in nominally pure Ar to 800 °C. In other words, this result confirms that the occurrence of reaction (3) is not only thermodynamically (see Fig. 10), but also kinetically, possible in the presence of a small concentration of oxygen in the atmosphere.

Fig. 12 exhibits the morphology of the SnO_2 powder obtained. SEM micrographs of the SnO_2 powder (Fig. 12a) demonstrate that the material has a wrinkled sheet-like morphology in the size range of several to several tens of micrometers. Furthermore, the bright field TEM images of the SnO_2 nanoparticles, such as shown in Fig. 12b and c, showed that the material consists of SnO_2 nanocrystals with sizes of 20–50 nm.

It was already known that $SnCl_2$ transforms to SnO_2 with sizes ranging from 20 to 120 nm at about 600 °C. It was further observed that these individual nanocrystals are integrated into larger single crystals when the sample is further heated to 800 °C [35]. The results of the current study shows that the nanocrystalline nature of the SnO_2 formed is retained even after heating to 800 °C, when $SnCl_2$ is heated with LiCl. The XRD pattern of the material obtained by heating LiCl–$SnCl_2$ to 1300 °C can be seen in Fig. 11b. The pattern is indexed to tetragonal phase of SnO_2 as the major phase and monoclinic Li_2SnO_3 as the minor phase. Fig. 12d illustrates SEM micrographs of the sample, demonstrating the presence of micron-sized particles with dimensions up to about 20 μm.

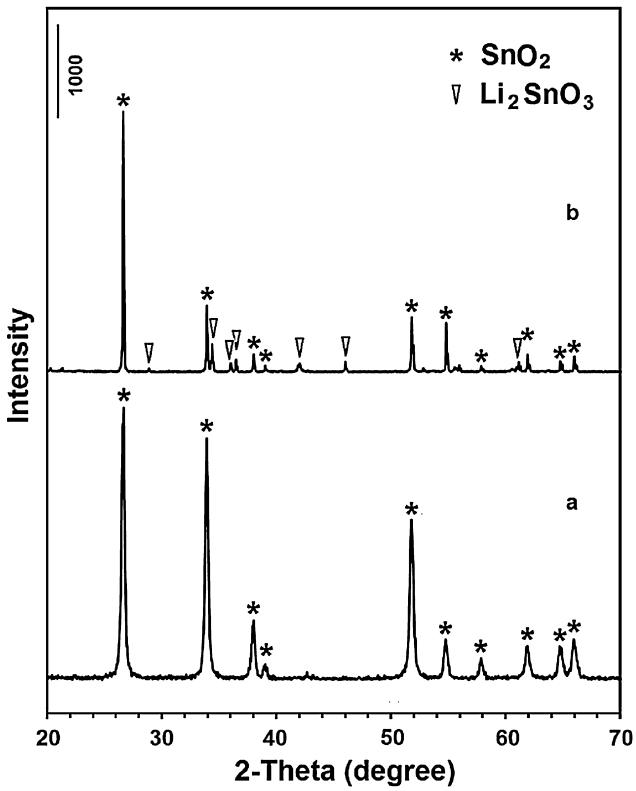

Fig. 11. XRD diffraction patterns of the mixture of LiCl and 30 wt% $SnCl_2$ heated to (a) 800 °C and (b) 1300 °C. The material obtained was then cooled to the room temperature under a flow of nominally pure Ar gas, washed with distilled water, and the suspension obtained was filtered and dried before the XRD analysis.

In our previous work, we studied the thermal behavior of LiCl [30]. It was found that LiCl undergoes a sequence of phase transitions when heated at the heating rate of 10 °C min^{-1}, as follows:

$$[LiCl \cdot H_2O]_{solid} \xrightarrow{93\,^\circ C} [LiCl]_{solid} \xrightarrow{608\,^\circ C} [LiCl]_{liquid} \xrightarrow{800\,^\circ C, H_2O} [LiCl - Li_2O]_{liquid} \quad (4)$$

According to (4), nominally anhydrous LiCl readily absorbs water from the ambient atmosphere to form a surface layer of lithium chloride hydrate. Upon heating, the hydrated LiCl is dehydrated at about 100 °C, and then melts at 608 °C. Molten LiCl is then partially hydrolysed at 800 °C to form LiOH, which subsequently decomposes to form Li_2O [30]. This finding was important because it implied the reactivity of molten LiCl, owing to the formation of Li_2O. We have recently shown that lithium oxides formed in molten LiCl can react with metal oxides such as Nb_2O_5 powders added to the molten salt to form $LiNbO_3$ crystals, introducing a fast and effective molten salt synthesis method [37].

Likewise, the formation of Li_2SnO_3 can also be explained according to phase transitions (3) and (4) based on the reaction between Li_2O (formed due to the hydrolysis of LiCl) and SnO_2 (formed due to the oxidation of $SnCl_2$), shown as reaction (5).

$$Li_2O + SnO_2 = Li_2SnO_3 \quad \Delta G^{\circ}_{1300\,^\circ C} = -508\,kJ \quad (5)$$

As mentioned, for the preparation of Sn-filled carbon nanostructures, the electrolysis of molten LiCl–$SnCl_2$ with graphite electrodes is conducted at high temperatures of greater than 700 °C [15,16]. It was also demonstrated that the temperature of molten salt could be locally raised considerably due to the exothermic reactions that took place [11].

The results obtained suggest that the formation of SnO_2 and Li_2SnO_3 occurs due to the exposure of LiCl–$SnCl_2$ salt mixture to atmospheres containing even a very small percentage of oxygen and moisture. The results also cast doubt on the hypothesis that Sn inside the cavity of carbon nanostructures partly reacts with oxygen during washing, drying or storage to form SnO_2, as pointed out in [15]. It is therefore important to evaluate the stability of Sn nanomaterials formed during the molten salt process against the subsequent washing and drying treatments.

3.4. Preparation of tin oxide free Sn-filled carbon nanostructures

The molten salt process was conducted at the same condition of that explained in Figs. 1 and 3, with only the exception that the process was conducted under a gas flow of high-purity argon containing 4% hydrogen. Under this reducing gas flow, therefore, the oxygen content of the atmosphere was supposed to be negligible. The mixture of Sn-containing carbon product and solidified salt was then washed with distilled water several times to dissolve the LiCl content. The suspension was then filtered and the filtrate was dried at 100 °C overnight. The XRD analysis of the final product is presented in Fig. 5c. Interestingly, no peak corresponding to SnO_2 can be observed in the pattern. This result further confirms that SnO_2 is formed during the molten salt process, if the atmosphere contains oxygen impurity. Moreover, the result indicates an excellent stability of the Sn-containing carbon nanostructures produced by this method against water and air. As shown in Fig. 5c, the sample also contained traces of Ni_3Sn_4 intermetallic phase. This phase was formed by the reaction between electrodeposited Sn and Ni introduced from the metallic components of the reactor.

3.5. Preparation of high-yield SnO_2-decorated CNTs

As explained in the previous sections, a scalable method was used to produce Sn-containing carbon nanostructures including Sn-filled CNTs and carbon nanoparticles, based on the electrolysis of molten LiCl and gradually added $SnCl_2$. It was shown that $SnCl_2$ is partially oxidized to form nano-single crystals of SnO_2 in a gas flow of argon containing 20 ppm oxygen. These nanocrystals decorate on the surfaces of CNTs in the final product. It was also shown in the Section 3.4 that the formation of SnO_2 nanoparticles could be avoided by using a reductive gas flow, preventing the oxidation of $SnCl_2$. As a logical extension of the results presented, we also explored the preparation of high-yield SnO_2-decorated CNTs using an Ar gas flow containing higher concentrations of oxygen. For this reason, the molten salt process was conducted at the same condition of those explained in the last sections (see Figs. 1 and 3) with the exception that the process was conducted under a gas flow of argon containing 2% oxygen. The XRD analysis of the product obtained is shown in Fig. 5b. As seen, the sample contains C and SnO_2 as the major phases and LiCl and Sn as the minor phases. TEM observations such as shown in Fig. 13 demonstrated that the CNTs formed are mostly decorated with SnO_2 in this sample.

As summary, we modified the molten salt method for the preparation of Sn-containing carbon nanostructures. The developed method uses continuous injection of $SnCl_2$ pellets into the molten salt during the electrolysis process. It was demonstrated that the molten salt process is sensitive to the presence of even small quantities of oxygen in the atmosphere, leading to the formation of tin oxide phases. In this case, SnO_2 was found to be formed as nano-single crystals attached to the surfaces of CNTs. Owing to their fascinating morphology, it would be interesting to study the relation between the quantity, size, morphology, and distribution of these SnO_2 nanocrystals to the oxygen concentration of the atmosphere in future work. It was demonstrated that the formation of tin oxide phases is avoided by using a reducing atmosphere. It was also found that Sn-filled carbon nanomaterials produced in molten salt is stable in air and water solutions. The results obtained provide a platform for future large-scale production of metal-filled carbon nanostructures in molten salts.

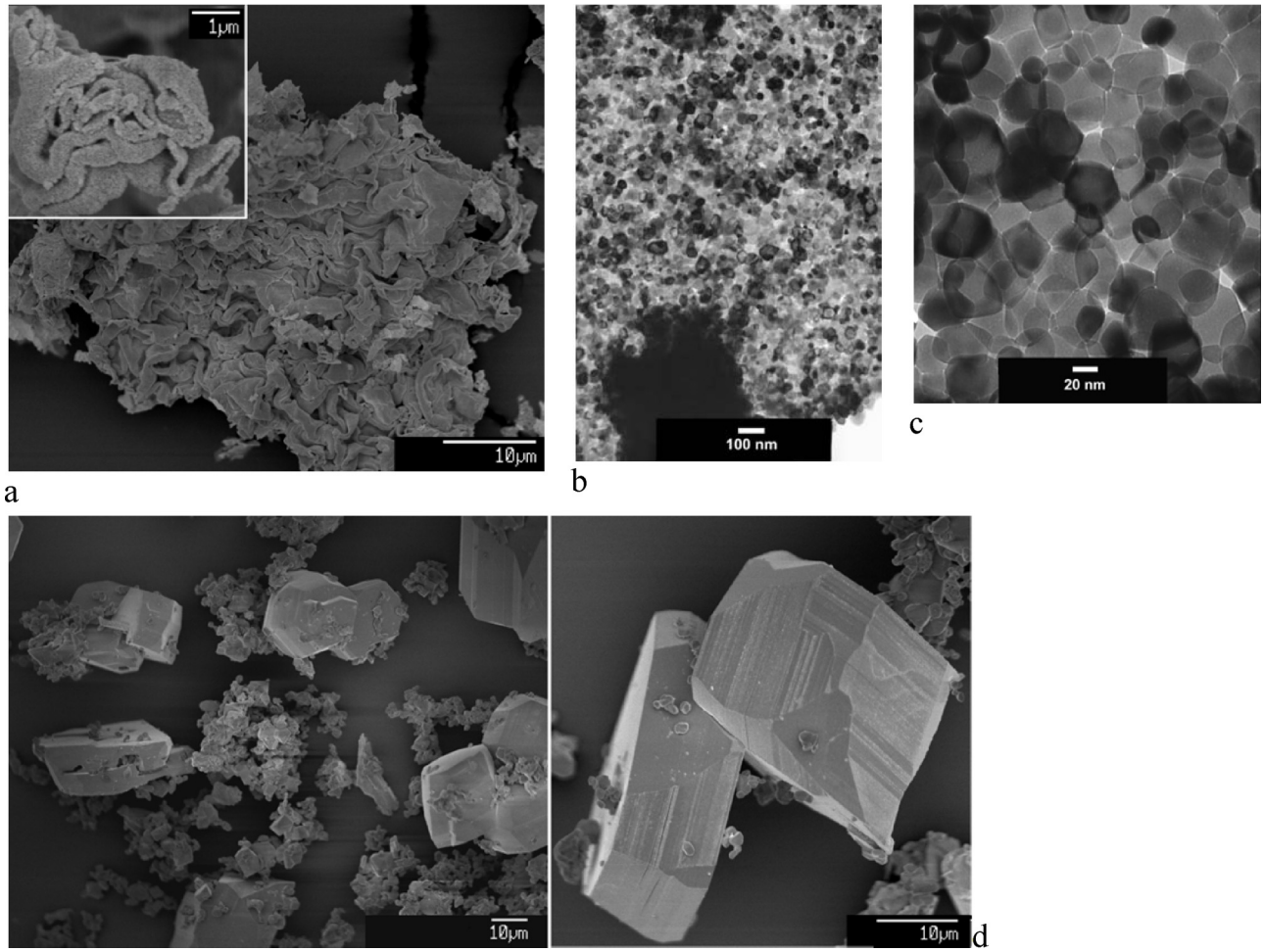

Fig. 12. (a) SEM and (b and c) TEM morphology of the SnO_2 powder obtained by heating a mixture of LiCl–30 wt% $SnCl_2$ in an argon flow to 800 °C and (d) 1300 °C.

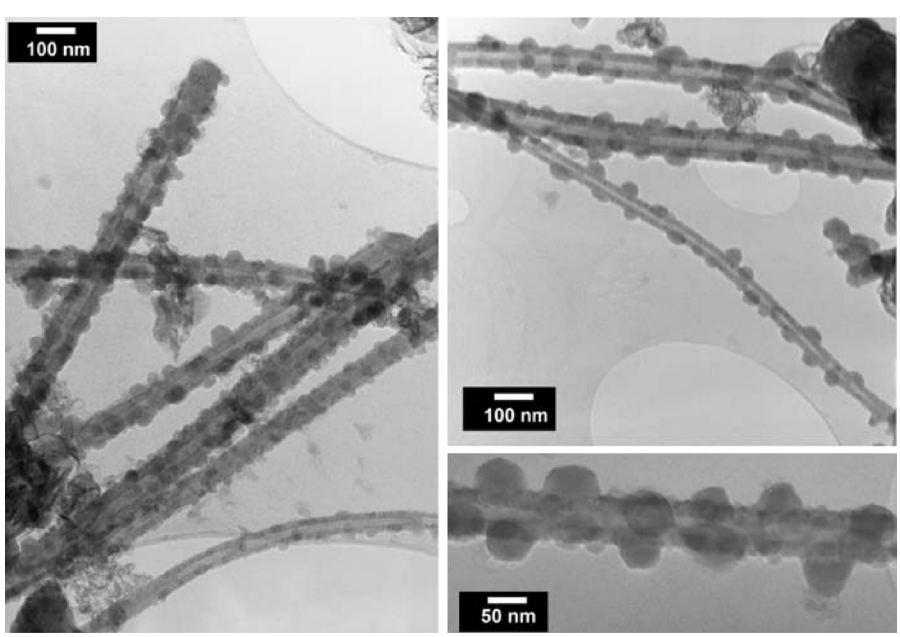

Fig. 13. TEM images of the sample prepared by 20 min electrolysis of molten LiCl – gradually added $SnCl_2$ in a gas flow of Ar – 2% O_2. The morphology observed could be characterized as mainly SnO_2-decorated CNTs.

4. Conclusion

The current method of producing Sn-containing carbon nanostructures in molten salts relies on the erosion of graphite cathodes during the electrolysis of pre-mixed LiCl and $SnCl_2$. However, the erosion of graphite electrodes does not occur if more than 2 wt% $SnCl_2$ is used. A modified method for molten salt preparation of Sn-containing carbon nanostructures was presented in this paper. In this method, $SnCl_2$ is gradually added to molten LiCl during the electrolysis. The modified method was evaluated by adding 7–30 wt% $SnCl_2$ without disruption of the erosion action. The product contained Sn-core carbon sheath nanostructures in addition to SnO_2-decorated CNTs. It was shown that the formation of SnO_2 nanocrystals is both energetically and kinetically favored in the presence of small quantities of oxygen in the atmosphere of the reactor. Formation of Li_2SnO_3 was also confirmed to be the result of the reaction between the SnO_2 nanocrystals and the Li_2O formed by the high temperature hydrolysis of molten LiCl. Formation of tin oxide phases was suppressed by conducting the process in a reducing atmosphere. On the other hand, high-yield SnO_2-decorated CNTs were synthesized by conducting the molten salt process in a gas flow of Ar-2% oxygen.

References

[1] A.R. Kamali, D.J. Fray, Molten salt corrosion of graphite as a possible way to make carbon nanostructures, Carbon 56 (2013) 121–131.
[2] X. Liu, M. Antonietti, Molten salt activation for synthesis of porous carbon nanostructures and carbon sheets, Carbon 69 (2014) 460–466.
[3] J. Sure, A.R. Shankar, S. Ramya, C. Mallika, U.K. Mudali, Corrosion behaviour of carbon materials exposed to molten lithium chloride–potassium chloride salt, Carbon 67 (2014) 643–655.
[4] Z. He, L. Gao, X. Wang, B. Zhang, W. Qi, J. Song, et al., Improvement of stacking order in graphite by molten fluoride salt infiltration, Carbon 72 (2014) 304–311.
[5] W.K. Hsu, J.P. Hare, M. Terrones, H.W. Kroto, D.R.M. Walton, P.J.F. Harris, Condensed-phase nanotubes, Nature 377 (1995) 687.
[6] G.Z. Chen, X.D. Fan, A. Luget, M.S.P. Shaffer, D.J. Fray, A.H. Windle, Electrolytic conversion of graphite to carbon nanotubes in fused salts, J. Electroanal. Chem. 446 (1998) 1–6.
[7] A.T. Dimitrov, G.Z. Chen, I.A. Kinloch, D.J. Fray, A feasibility study of scaling-up the electrolytic production of carbon nanotubes in molten salts, Electrochim. Acta 48 (2002) 91–102.
[8] C. Schwandt, A.T. Dimitrov, D.J. Fray, The preparation of nano-structured carbon materials by electrolysis of molten lithium chloride at graphite electrodes, J. Electroanal. Chem. 647 (2010) 150–158.
[9] C. Schwandt, A.T. Dimitrov, D.J. Fray, High-yield synthesis of multi-walled carbon nanotubes from graphite by molten salt electrolysis, Carbon 50 (2012) 1311–1315.
[10] A.R. Kamali, C. Schwandt, D.J. Fray, Effect of the graphite electrode material on the characteristics of molten salt electrolytically produced carbon nanomaterials, Mater. Charact. 62 (2011) 987–994.
[11] A.R. Kamali, D.J. Fray, Towards large scale preparation of carbon nanostructures in molten LiCl, Carbon 77 (2014) 835–845.
[12] W.K. Hsu, S. Trasobares, H. Terrones, M. Terrones, N. Grobert, Y.Q. Zhu, W.Z. Li, R. Escudero, J.P. Hare, H.W. Kroto, D.R.M. Walton, Electrolytic formation of carbon-sheathed mixed Sn–Pb nanowires, Chem. Mater. 11 (1999) 1747–1751.
[13] M. Terrones, W.K. Hsu, A. Schilder, H. Terrones, N. Grobert, J.P. Hare, et al., Novel nanotubes and encapsulated nanowires, Appl. Phys. A 66 (1998) 307–317.
[14] Q. Xu, C. Schwandt, D.J. Fray, Electrochemical investigation of lithium and tin reduction at a graphite cathode in molten chlorides, J. Electroanal. Chem. 562 (2004) 15–21.
[15] R.D. Gupta, C. Schwandt, D.J. Fray, Preparation of tin-filled carbon nanotubes and nanoparticles by molten salt electrolysis, Carbon 70 (2014) 142–148.
[16] R.D. Gupta, The electrochemical production of tin filled carbon nanotubes and their use as anode materials in lithium-ion batteries (PhD thesis), University of Cambridge, Department of Materials Science and Metallurgy, 2008.
[17] Y. Wang, M. Wu, Z. Jiao, J.Y. Lee, Sn@CNT and Sn@C@CNT nanostructures for superior reversible lithium ion storage, Chem. Mater. 21 (2009) 3210–3215.
[18] L. Jankovic, D. Gournis, P.N. Trikalitis, I. Arfaoui, T. Cren, P. Rudolf, Carbon nanotubes encapsulating superconducting single-crystalline tin nanowires, Nano Lett. 6 (2006) 1131–1135.
[19] X. Hou, H. Jiang, Y. Hu, Y. Li, J. Huo, C. Li, In situ deposition of hierarchical architecture assembly from Sn-filled CNTs for lithium-ion batteries, ACS Appl. Mater. Interfaces 5 (2013) 6672–6677.
[20] T. Tokunaga, T. Kanematsu, T. Ito, T. Ota, Y. Hayashi, K. Sasaki, et al., Fabrication of tin-filled carbon nanofibres by microwave plasma vapour deposition and their in situ heating observation by environmental transmission electron microscopy, Nanoscale Res. Lett. 8 (2013) 302.
[21] T.P. Kumar, R. Ramesh, Y.Y. Lin, G.T.K. Fey, Tin-filled carbon nanotubes as insertion anode materials for lithium-ion batteries, Electrochem. Commun. 6 (2004) 520–525.
[22] Y. Zhong, M. Yang, Xianlong, Z.J. Wei, Z. Zhou, Towards excellent anodes for Li-ion batteries with high capacity and super long lifespan: confining ultrasmall Sn particles into N-rich graphene-based nanosheets, Part. Part. Syst. Char. (2014), http://dx.doi.org/10.1002/ppsc.201400105.
[23] Z. Tan, Z. Sun, H. Wang, Q. Guo, D. Su, Fabrication of porous Sn–C composites with high initial coulomb efficiency and good cyclic performance for lithium ion batteries, J. Mater. Chem. A 1 (2013) 9462–9468.
[24] Y. Xu, Q. Liu, Y. Zhu, Y. Liu, A. Langrock, M.R. Zachariah, C. Wang, Uniform nano-Sn/C composite anodes for lithium ion batteries, Nano Lett. 13 (2013) 470–474.
[25] J. Guo, Z. Yang, L.A. Archer, Aerosol assisted synthesis of hierarchical tin-carbon composites and their application as lithium battery anode materials, J. Mater. Chem. A 1 (2013) 8710–8715.
[26] I. Meschini, F. Nobili, M. Mancini, R. Marassi, R. Tossici, A. Savoini, et al., High-performance Sn@carbon nanocomposite anode for lithium batteries, J. Power Sources 226 (2013) 241–248.
[27] A.R. Kamali, D.J. Fray, Tin-based materials as advanced anode materials for lithium ion batteries: a review, Rev. Adv. Mater. Sci. 27 (2011) 14–24.
[28] X. Tao, L. Dong, W. Zhang, X. Zhang, J. Cheng, H. Huang, et al., Controllable melting and flow of b-Sn in flexible amorphous carbon nanotubes, Carbon 47 (2009) 3122–3127.
[29] A. Roine, Outokumpu HSC chemistry for windows-chemical reaction and equilibrium software with extensive thermochemical database: Version 5.0, Outkumpu Research Oy Information Service, Finland, 2002.
[30] A.R. Kamali, D.J. Fray, C. Schwandt, Thermokinetic characteristics of lithium chloride, J. Therm. Anal. Calorim. 104 (2011) 619–626.
[31] A.R. Kamali, G. Divitini, C. Schwandt, D.J. Fray, Correlation between microstructure and thermokinetic characteristics of electrolytic carbon nanomaterials, Corros. Sci. 64 (2012) 90–97.
[32] Y. Zhang, S. Cui, J. Chang, L.E. Ocola, J. Chen, Highly sensitive room temperature carbon monoxide detection using SnO_2 nanoparticle-decorated semiconducting single-walled carbon nanotubes, Nanotechnology 24 (2013) 025503.
[33] J.Y. Lin, M.H. Chou, Y.C. Kuo, Rapid synthesis of tin oxide decorated carbon nanotube nanocomposities as anode materials for lithium-ion batteries, J. Alloys Compd. 589 (2014) 472–478.
[34] A.R. Kamali, D.J. Fray, Solid phase growth of tin oxide nanostructures, Mater. Sci. Eng. B 177 (2012) 819–825.
[35] A.R. Kamali, G. Divitini, C. Ducati, D.J. Fray, Transformation of molten $SnCl_2$ to SnO_2 nano-single crystals, Ceram. Int. 40 (2014) 8533–8538.
[36] A.R. Kamali, Thermokinetic characterisation of Tin(II) chloride, J. Therm. Anal. Calorim. 118 (2014) 99–104.
[37] A.R. Kamali, D.J. Fray, Preparation of lithium niobate particles via reactive molten salt synthesis method, Ceram. Int. 40 (2014) 1835–1841.